Proceedings of the 21st ICSMGE, Vienna, Austria, 14 – 19 June 2026. Pistrol, Adam & Schweiger (eds.)
Published by: ÖGG, Austrian Society for Geomechanics, Salzburg, Austria, ISBN 978-3-9503898-4-5
https://doi.org/10.53243/ICSMGE2026-799

Flow-Sediment-Foundation Interaction: From Flume to Centrifuge Modeling

Ahmad Klait, Mark Adler, **Majid Ghayoomi**
Department of Civil and Environmental Engineering, University of New Hampshire, Durham, USA, majid.ghayoomi@unh.edu

Seyedalireza Mirghafouri, Ali Farhadzadeh
Department of Civil Engineering, Stony Brook University, Stony Brook, USA, ali.farhadzadeh@stonybrook.edu

Tian-Jian Hsu
Department of Civil and Environmental Engineering, University of Delaware, Newark, USA, thsu@udel.edu

ABSTRACT:

This study investigates wave-induced excess pore pressure (EPP) development and wave–soil–structure interaction in sandy coastal environments using a dual-scale physical modeling approach. Using large-scale flume experiment, solitary wave loading was simulated on a sandy seabed with and without a shallow embedded foundation. Results showed increased wave heights significantly amplified excess pore pressures and deepened pressure transmission, while the presence of a shallow foundation altered pressure peaks and induced complex seepage gradients influencing soil stability. Although pore pressures remained below liquefaction thresholds, observed pore pressure gradients and wave-induced forces caused momentary structural instability under stronger waves. To complement these findings, a novel centrifuge modeling system was developed at the University of New Hampshire, featuring an integrated wave maker and load actuator designed to replicate wave-soil-structure interactions under scaled stress conditions. Preliminary centrifuge tests demonstrated the system's capability to reproduce excess pore pressure cycles and foundational movements such as rocking and settlement under steady wave loading. This dual-model framework leverages the strengths of large-scale realistic wave simulation and stress-accurate centrifuge modeling, overcoming individual limitations to provide comprehensive insights into coastal foundation behavior under dynamic hydrodynamic loading.

KEYWORDS: Coastal Foundations, Wave-soil-structure interaction, Excess pore pressure, Flume experiments, Centrifuge modeling.

1 INTRODUCTION

Wave-induced excess pore pressure (EPP) accumulation and upward-directed vertical seepage gradients driven by coastal flooding and other hydrodynamic processes can destabilize soils in coastal zones where terrestrial land meets submerged environments, posing risks to coastal infrastructure (Anderson et al., 2017; Stark, 2017; Paldor et al., 2022; Chen et al., 2024). Extreme wave loading can induce excess pore pressures that either exceed the initial effective stress (Seed and Rahman, 1978) or generate upward seepage forces surpassing the critical hydraulic gradient of the soil (Terzaghi et al., 1996), potentially leading to liquefaction, piping, or quick conditions (Knappett et al. 2012; Sumer and Fredsøe 2006). These processes combined with hydrodynamic loading on coastal foundations/structures will result in complex wave-soil-structure interaction. Thus, understanding the interplay among waves, sediment, and structures, along with the spatial and temporal variation of pore water pressure, is crucial for evaluating the stability of coastal infrastructure (Jeng, 2003).

Experimental studies have provided valuable insights into the dynamic response of soil beds under wave action, particularly focusing on pressure buildup and the onset of liquefaction (e.g., Zhang et al., 2020; Li, Gao and Yang, 2021). Field investigations have also contributed to understanding in-situ pore pressure responses and hydraulic gradients under natural wave environments (e.g., Mory et al., 2007; Michallet, Mory and Piedra-Cueva, 2009; Xu et al., 2021; Marry and Foster, 2024). Numerical modeling has also been used to simulate the dynamic response of coastal soils and systems under wave loading (e.g., Dunn et al., 2006; Young et al., 2009; Scholtès et al., 2015). In parallel, analytical methods have been developed to describe wave-induced pressure distributions (e.g., Sayedmasoud and Ghayoomi, 2020; Fu et al., 2025). Moreover, the vast majority of existing research has focused on offshore structures such as breakwaters, pipelines, and caissons, primarily using large-scale flume experiments, numerical simulations, and field observations (Dunn et al., 2006; Mory et al., 2007; Michallet, Mory and Piedra-Cueva, 2009). In contrast, there has been limited emphasis on nearshore soil response, particularly in the presence or absence of shallow foundations supporting coastal infrastructure, such as low-lying residential buildings. Additionally, very few studies have utilized centrifuge physical modeling in coastal contexts (e.g., Exton et al. 2019).

To address these gaps and complexities of wave–soil–structure interaction in near-coastal environments, this study adopts a dual-model framework that combines large-scale flume testing and a novel centrifuge-based physical modeling. Each technique offers unique strengths: the flume enables testing under realistic wave conditions and allows direct observation of fluid-structure-soil responses at near-prototype scale, while the centrifuge modeling enables replication of high-stress field conditions and allows for efficient scaling of soil behavior within a controlled laboratory setting.

Despite these advantages, both methods also present inherent limitations. Flume testing, while effective for simulating realistic hydrodynamic conditions, is limited by scale effects and sediment layer thickness constraints. On the other hand, centrifuge modeling, although capable of achieving correct stress scaling and capturing detailed soil response, may face challenges related to wave generation, particularly for storm- or tsunami-like conditions, and inability to simulate long gentle slope considering the limited space within the centrifuge platform. Additional challenges include instrumentation complexities that can exist in both methods. Hence, the complementary use of both modeling techniques in this study will address the aforementioned gaps and leverage their respective strengths to provide a more comprehensive understanding of the underlying mechanisms. This paper provides an introductory approach to this dual-scale physical

modeling campaign presenting the flume experiment setup and the review of the outcome, and the new wave maker setup and performance. Although other types of waves are tested, data from solitary waves in flume and steady state wave calibration for centrifuge are presented. The testing campaign included both free field soil layer and also embedded foundation. The paper is divided into two sections one describing the flume experiments and results and the other presenting the centrifuge setup and what we learned and plans forward.

2 WAVE FLUME EXPERIMENTS

2.1 *Experimental Program*

Physical modeling experiments were conducted at the O.H. Hinsdale Wave Research Laboratory at Oregon State University, utilizing its large-scale wave flume. The flume measures 104 meters in length, 3.67 meters in width, and 4.67 meters in height, and includes a sand-filled pit that simulates the seabed. Figure 1 provides a truncated top-view layout of the facility, identifying several key features: (i) a sand trench measuring 1.45 m in depth, 3.67 m in width, and 7.32 m in length, located between bays 8 and 10; (ii) a centrally placed concrete column weighing 4.8 tons with a square cross-section of 1 m × 1 m and a height of 2.67 m, situated in bay 9. Notably, the large flume also features other components that are not fully detailed due to space constraints, such as (iii) a piston-type wave generator located at the upstream (left) end, and (iv) a concrete coastal slope with a 1:12 inclination installed between bays 4 and 8 (highlighted in light yellow in Figure 1). Additionally, the flume incorporates a transition from slope to horizontal bed between bays 10 and 15 (not shown), followed by a return to a 1:12 slope from bays 15 to 19, designed to reduce wave reflections during the rundown phase (green section in Figure 1). Figure 2 illustrates the sensor arrangement, which is discussed in more detail in subsequent sections.

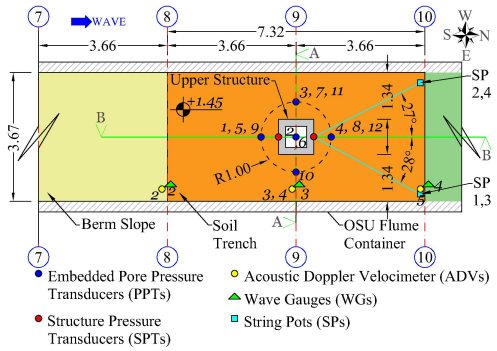

Figure 1. Truncated top view of the experimental setup, highlighting instrumentation layout All dimensions are in meters.

2.2 *Experimental Conditions and Procedure*

This study involved two primary testing configurations: (1) a condition incorporating a shallow foundation within the soil; Figures 1 and 2 are associated with this scenario; however, the free-field tests utilized the same instrumentation layout and general setup. Both configurations, discussed herein, were subjected to solitary wave (SW) loading with heights of 60 cm (SW60) and 110 cm (SW110), generated following the procedures outlined by Hughes (1993). The SW60 wave, which did not break before reaching the test section, is considered non-breaking, whereas the SW110 wave exhibited plunging behavior upon interacting with the structure. In tests involving the soil–foundation interaction, two embedment depths were examined—35 cm and 50 cm. A constant still water level of 2 m from the flume base was maintained across all tests. Specifically, this resulted in a local still water depth of 55 cm in the onshore region around the structure. A full overview of test conditions is presented in Table 1.

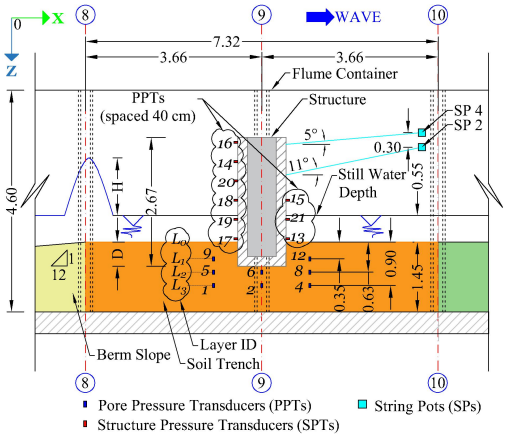

Figure 2. Truncated longitudinal cross-section (Section B-B) of the experimental setup, illustrating different heights of deployed instrumentation. All dimensions are in meters.

Table 1. Overview of Conducted Large-Scale Flume Tests.

Test #	Test ID	Test Label
1	SW_WH60_h200_hs55_NS	WH60
2	SW_WH110_h200_hs55_NS	WH110
3	SW_WH60_h200_hs55_WS_D35	WH60 (D35)
4	SW_WH110_h200_hs55_WS_D35	WH110 (D35)
5	SW_WH110_h200_hs55_WS_D50	WH110 (D50)

Note: SW = Solitary wave; WH = Wave height; h = Offshore still water level (S.W.L) from the base of the flume; hs = Still water level around structure; NS = No structure; WS = With structure; D = Structure embedment depth.

A sand trench was first constructed by placing sand within the specified area, ensuring the proper installation of pore pressure transducers (PPTs) at three horizontal layers located at depths of 35 cm, 62.5 cm, and 90 cm below the mudline (Figure 2). The flume was gradually filled with water to reach a still water level (S.W.L.). Water was introduced using two pumps simultaneously, one positioned at the southern upstream end near the wavemaker (bay 3) and the other at the northern downstream end (bay 22) (not displayed in Figure 1). Employing both pumps concurrently was crucial to avoid disturbing the sand bed, which could have happened if filling occurred from only one side. Once filled, time was allowed for the S.W.L. to stabilize while sensors were calibrated. Subsequently, the wavemaker was activated, taking approximately 30 seconds to produce the desired wave conditions. After each test, the flume was slowly drained until the water level dropped to the midpoint of the coastal concrete slope, revealing the sand pit surface. The soil deposit was then restored and leveled to its initial state. For soil-foundation tests, the structure was installed after compacting the soil to a height of 110 cm above the flume base, corresponding to an embedment depth of 35 cm from the mudline (or 50 cm for deeper embedment case). Notably, solitary waves were adopted to simulate tsunami-like flow conditions, as long-period tsunami waves can evolve into soliton trains during nearshore propagation (Sriram et al., 2016). Previous studies have shown

that tsunami run-up and bore impact resemble the behavior of solitary or dam-break waves (Chanson, 2006). The use of piston-generated solitary waves therefore provides a practical and widely accepted laboratory approach for reproducing tsunami-induced hydrodynamic loading (Sriram et al., 2016).

2.3 *Instrumentation and Monitoring*

Two pairs of string potentiometers (SPs), totaling four units, were installed on the northwest (NW) and northeast (NE) walls of the large flume, as depicted in Figure 1 (highlighted with cyan rectangles). Each pair was vertically spaced by 30 cm, with wiring directed toward the structure's centerline to accurately capture its movement under wave-induced dynamics. For the embedment depth of 50 cm, the SPs were inclined at angles of 27° on the NW side (SP2 and SP4) and 28° on the NE side (SP1 and SP3) relative to the x–y plane, as shown in Figure 1. Additionally, inclinations relative to the x–z plane were about 11° for SP1 and SP2, and approximately 5° for SP3 and SP4, illustrated in Figure 2.

To track pore pressure variations, a set of embedded PPTs were placed within the soil matrix. A network of 12 non-flush embedded pore pressure sensors (PDCR1830) recorded the spatial and temporal changes of pore water pressure inside the sand trench (Figure 1). These PPTs were positioned 1 meter offset from the structure's centerline (bay 9, Figure 1) at multiple locations including the South (upwave), North (downwave), West, East, and directly beneath the foundation. The distribution of PPTs is illustrated in Figure 1 with blue circles: three on the west side (PPT 3, 7, 11), three to the south (PPT 1, 5, 9), three on the north (PPT 4, 8, 12), one on the east side (PPT 10), and two beneath the foundation (PPT 2, 6). A vertical cross-section of the deployed PPTs along section B-B is shown in Figure 2.

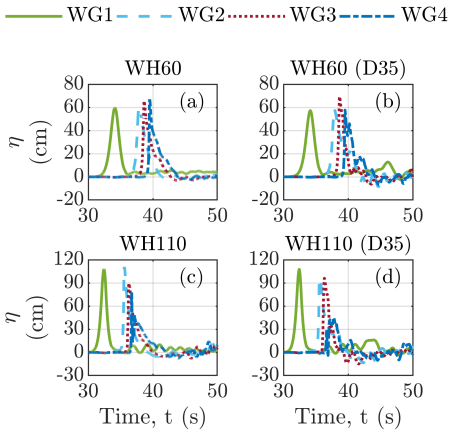

Figure 3. Recorded solitary wave heights (η) from four wave gauges (WG1–WG4) across five experimental cases: (a) WH60, (b) WH60 with 35 cm embedment, (c) WH110, (d) and WH110 with 35 cm embedment. The WH110 with 50 cm embedment isn't displayed due to similarities with panel (d).

Furthermore, five acoustic Doppler velocimeters (ADVs) were installed along the east wall of the flume to measure velocity components—shoreward, lateral, and vertical—at bays 3, 8, 9, and 10, indicated by yellow circles in Figure 1 (showing only those at bays 8, 9 and 10 for space constraints). To monitor the water surface elevation relative to the still water level (S.W.L.) as waves traveled along the flume, four wave gauges (WGs) were positioned at various points, marked as green triangles in Figure 1 (WG1 isn't displayed for space constraints). Time-series data representing the evolution of solitary wave (SW) heights recorded by these wave gauges (WG1–WG4) for all tests summarized in Table 1 are presented in Figure 3.

In addition, nine flush-mounted structure pressure transducers (SPTs) were installed on the structure itself, spaced at 40 cm intervals—six on the seaward side and three on the leeward side (Figure 2)—to capture wave impact forces and aid in evaluating structural stability through pressure measurements. Actual deployment photographs of the SPs on the seaward face, as well as the wave gauges and SPTs, are provided in Figure 4(a–c).

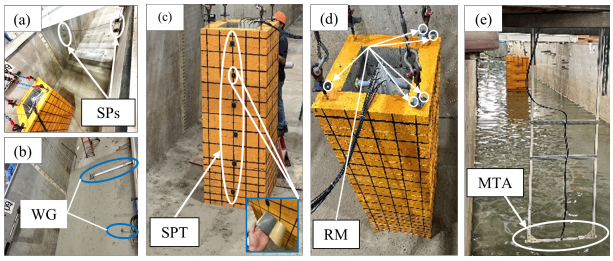

Figure 4. Field deployment of key instruments, including: (a) string potentiometers, (b) a wave gauge, (c) pressure transducers on the structure shielded with elastic material (in red), (d) reflective markers from the Qualisys motion tracking system, and (e) the multi-transducer array (MTA).

A Qualisys motion capture system, featuring high-resolution cameras and reflective markers (RMs), was also employed to precisely track structural motion (Figure 4d). To map changes in soil surface elevation, a Light Detection and Ranging (LiDAR) system was used, enabling a detailed assessment of scour, sediment transport, and deposition. Additionally, a Multi-Transducer Array (MTA) system was utilized as a secondary method to monitor bathymetric variations before and after each individual test, as shown in Figure 4(e). While each of these instruments contributes valuable data on system behavior, this paper emphasizes the results obtained from the PPTs and WGs, with selected references to SPT and SP data to support our discussion.

2.4 *Soil Material Properties*

According to the Unified Soil Classification System (USCS), the tested soil falls under the SP category, identifying it as poorly graded sand. Dry sieve analysis revealed characteristic particle sizes of $D_{10} = 0.17\,mm$, $D_{30} = 0.20\,mm$, and $D_{50} = 0.22\,mm$. From these values, the uniformity coefficient (C_u) and coefficient of curvature (Cc) were determined to be 1.36 and 1.02, respectively.

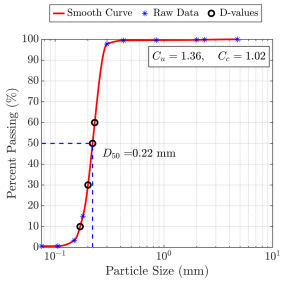

Figure 5. Grain size distribution curve of the tested sand

The grain size distribution is illustrated in Figure 5. Using the empirical relationship proposed by (MacRobert, Bernstein and Nchabeleng, 2019), which links dynamic penetration rate (mm/blow) to relative density (D_r), results from dynamic cone penetration (DCP) tests at the site indicated an initial relative density close to 60%.

2.5 *Foundation*

The structure, standing 2.67 m tall with 20 cm thick walls, featured a shallow square foundation measuring 1 m in width

and 15 cm in thickness. The structure was built using hollow concrete masonry blocks, stacked in approximately 12 horizontal layers to achieve the desired height. To improve its resistance to wave loading, the hollow core—extending up to 2 m in height—was filled with material, bringing the total weight to around 4.8 tons with the fill and approximately 3.2 tons without it. Reinforcing bars were installed around the perimeter and vertically through the hollow blocks to help counteract tensile forces generated by wave action. Space within the hollow section was also reserved for installing structure-mounted pressure transducers (SPTs), which were secured via embedded pipes before adding the fill material. For optical motion tracking, the exterior was painted orange and marked with a black grid pattern—spaced at 20 cm intervals both vertically and horizontally, and 10 cm below the still water level. An image sequence of the breaking SW110 hitting the structure is shown in Figure 6 (a-d) causing momentary instability for this breaking wave. Such instability was not observed for SW60.

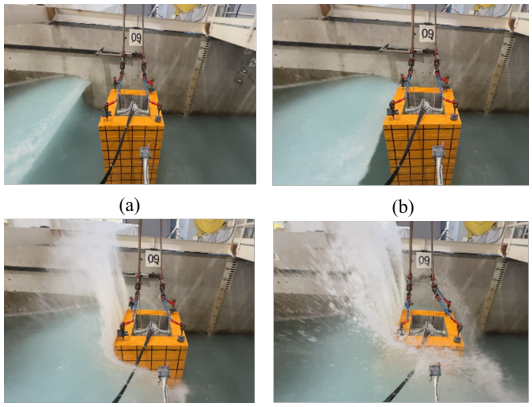

Figure 6. Image sequence of wave-structure interaction.

2.6 *EPP Evolution*

Figure 7 (a-d) shows the evolution of EPP head at the center location (bay 9) for five test scenarios (Table 1). The first EPP peak with its time of occurrence in addition to the followed drop were used to evaluate the wave-induced response. The first EPP peak increased consistently with wave height under free-field conditions (Figure 7, a-b). At 62.5 cm depth (PPT6), values rose from 1.06 cm to 2.28 cm (~115% increase). At 90 cm depth (PPT2), values rose from 1.20 cm to 2.15 cm (~79%). This trend indicates stronger loading and deeper pressure transmission under larger waves. Notably, no drop in EPP was observed under free-field conditions following the first recorded EPP. However, in soil-foundation tests under SW110, an EPP drop was observed following the first EPP peak (Figure 7, c-d). In essence, under soil-foundation conditions, the first EPP peak under SW110 impact at PPT6 showed a moderate increase (0.41 cm to 0.54 cm, ~32%) (Figure 7, c). At PPT2, however, the first EPP peak decreased (0.72 cm to 0.27 cm), reflecting complex wave-structure interactions and energy dissipation that reduce pressure transmission, especially at depth (Figure 7, d). Increasing embedment from D35 to D50, under SW110 impact, slightly reduced the first EPP peak (0.54 cm → 0.47 cm) at 62.5 cm depth (PPT6), indicating lower chance of potential liquefaction. the subsequent EPP drop magnitude also became slightly smaller, (–88.28 cm → –75.25 cm).

However, at PPT2 (90 cm), under same loading conditions, the first EPP peak increased markedly (0.27 cm → 1.04 cm) at that instant, indicating more susceptibility to exceeding the liquefaction threshold (Figure 7, d). At the instant of wave impact, however, the following EPP drop became more negative (–24.98 cm → –82.91 cm), suggesting more stability in deeper embedment (Figure 7, d).

Notably, all recorded EPP head responses (Figure 7, a-d) fell below the critical limit for liquefaction during both the free-field and soil-foundation experiments.

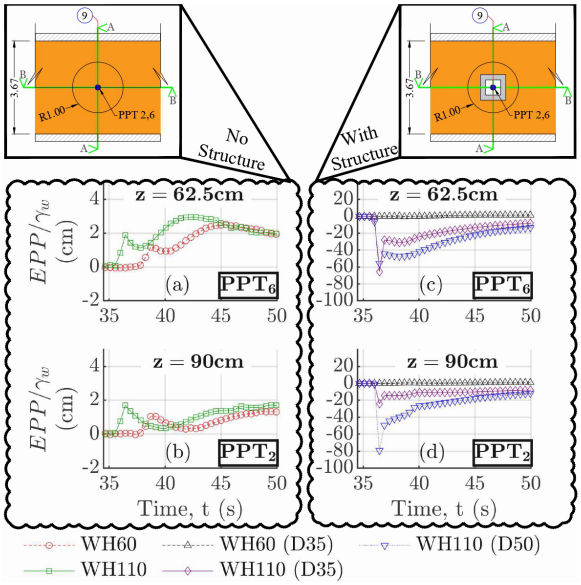

Figure 7. Free-filed and soil-foundation testing conditions: temporal and spatial evolution of excess pore pressure head $\left(EPP/\gamma_w\right)$ at the center location (beneath foundation, bay 9).

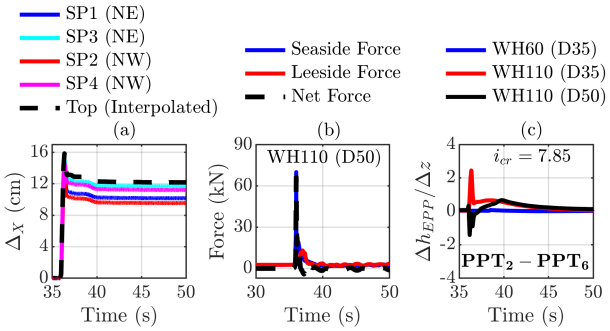

Figure 8. (a) recorded displacement from 4 SPs; (b) computed wave-induced force from installed SPTs under WH110 (D50) test conditions; (c) temporal development of the excess pore pressure gradient $\left(\frac{\Delta h_{EPP}}{\Delta z}\right)$ at the center location (bay 9) under soil-foundation condition.

Although classic liquefaction was not observed, the differential EPP drop within layers indicated the potential influence of upward seepage gradients within the soil. These upward-directed gradients can weaken effective stress and induce localized instability, especially in sandy soils. This motivation was also supported with noticeable observation both on site and through recorded significant horizontal displacement (~15.35 cm, Figure 8(a)) at the top of the structure, suggesting a possible interplay between upward flow and foundation movement under wave loading due to the net wave-induced impact force computed from SPTs as 66.44 KN (Figure 8(b)) under WH110 (D50) test condition. A summary of the seepage-induced instability investigation is provided in Figure 8(c) which shows the evolution of EPP gradients at the center location (bay 9) along with the critical liquefaction threshold shown as $i_{cr} = 7.85$.

Figure 8(c) provides key observations which include that the presence of the structure under higher wave embedment significantly alters the EPP gradient. However, lower wave

heights didn't induce high gradients where the recorded was 0.05 at around 38 seconds (WH60 (D35)), suggesting small localized pore pressure effects at the center of the structure. Alternatively, for WH110 (D35), a dramatic increase to 2.41 at 36 seconds is observed, indicating a strong pore pressure gradient likely induced by wave-structure interaction.

At a higher embedment depth of 50 cm under the SW110 wave height, the EPP gradient shifts negatively to -1.37 at 36 seconds, suggesting a reversal or redistribution of hydraulic gradients potentially due to deeper structural effects on subsurface flow paths. These results demonstrate the critical influence of both wave height and structural embedment depth on the development and evolution of pressure gradients in sandy seabed.

3 CENTRIFUGE MODELING

3.1 *Model Design*

To complement the large-scale flume experiments, an innovative centrifuge testing platform has been designed and developed at the University of New Hampshire for modeling wave–soil–structure interaction in nearshore environments. The current setup includes a custom-designed container and integrated wave generation system, both calibrated and validated through initial test series.

The centrifuge container consists of a soil trench with saturation network, a wavemaker piston and actuator, a wave absorber system, model structure, and a load actuator system (Figure 9, a-b). The centrifuge wavemaker was designed to meet the following criteria: (1) minimize boundary effects when the foundation is placed in the soil trench; (2) provide a sufficient range of wavemaker actuator stroke and frequency, including the ability to generate steady-state waves ,; (3) position the wave generator far enough from the structure to avoid disturbance and ensure correct wave simulation; (4) incorporate a slotted/partitioned wave absorber with appropriate spacing and partitioning design; and (5) satisfy all scaling factors governing centrifuge modeling of the soil system.

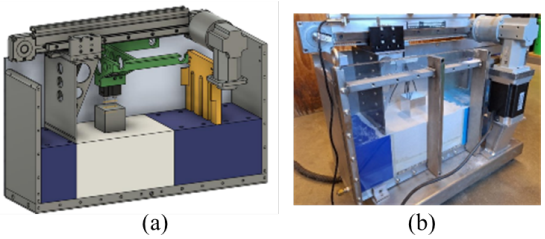

(a) (b)

Figure 9. (a) Schematic and (b) image of the newly developed centrifuge modeling system.

The system is calibrated for performance and input/output data validity. In one preliminary effort, a soil trench with dimensions of 24.4 cm (length), 15.2 cm (width), and 12.7 cm (depth) was prepared while a 5×5×5 cm model structure was placed atop. The SP-fine silica sand was used at 33% relative density. Waves at frequency of 9.26 Hz and at strokes of 3, 4, and 5 cm were generated. Water was added to a height of 3 cm above the soil bed and the wave absorber was offset from the back wall by 10 cm. A schematic of the PPTs placed under the structure is shown in Figure 10. Similar configuration was repeated for no-structure tests.

Focusing for example, on PPT2 under a steady-state wave with a 3 cm stroke, Figure 11 shows the cycles of pore pressure during steady state wave generation. Since the tests were performed over 20 seconds which will include about 193 cycles the figure shows three inserts from three different periods of 1 second.

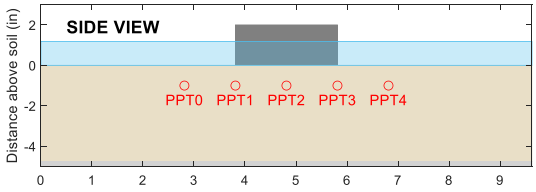

Figure 10. cross-section schematic showing the deployed PPTs beneath the structure

The data is shown for both free-field and the case with model structure. The data clearly show the difference in generated pore water pressure between the free-field and soil-structure case at different times both in terms of cycled amplitude and residual accumulated pore pressure.

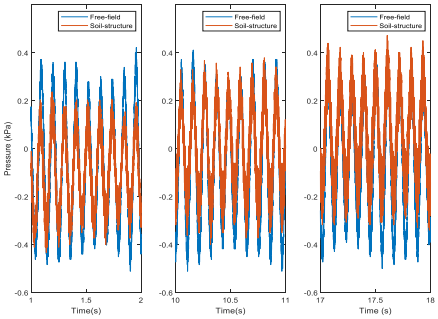

Figure 11. Pressure vs. time data at PPT2 for 3 cm stroke.

These preliminary tests demonstrated the system's ability to reproduce excess pore pressure development, soil–structure interaction responses, and foundational movements such as rocking and settlement under progressive wave loading. Especially, the setup has the capacity to simultaneously load and physically rock the system while the wave action is occurring. Building upon this baseline, ongoing efforts are now focused on expanding the system's capabilities. This includes modification to wave absorber for better performance and studying coupled hydrodynamical. Additionally, further testing with steady waves and solitary type waves are underway.

4 CONCLUSIONS

This study examined the development of excess pore pressure (EPP) in a sandy seabed subjected to wave loading using large-scale flume tests under free-field and soil–foundation conditions and inside the newly developed centrifuge wavemaker container. Results from the flume tests show that increasing wave height significantly amplifies the magnitude and depth of excess pore pressure transmission compared to lower wave height conditions. Introducing a shallowly embedded structure reduced the first peak of the excess pore pressure at depth, indicating energy dissipation and altered wave-structure interaction, while deeper embedment caused higher first peak of excess pore pressure and more negative post-peak drops in excess pore pressure. This is combined with potential upward seepage forces. Gradient analysis revealed that the produced upward-directed gradient, indicating instability, but less of that in deeper embedment case with downward-directed gradients at times. Despite these effects, all measured values remained below liquefaction or seepage failure thresholds.

Additionally, the wave-induced forces and the pore pressure-induced reduction in effective stress collectively introduced momentary instability in the structure under the stronger waves. Further, the centrifuge wavemaker showed

promise in simulating wave action and the impact of wave-soil-structure interaction, which can complement the shortcomings of 1-g soil models.

5 ACKNOWLEDGEMENTS

This research was funded by the National Science Foundation through Grants No. 2050808 and 2050798. The authors also express their gratitude to the technical staff and undergraduate volunteers at the O.H. Hinsdale Wave Research Laboratory at Oregon State University and Noah McAdam from UNH Technical Service Center.

6 REFERENCES

Abdoun, T., Gonzalez, M.A., Thevanayagam, S., Dobry, R., Elgamal, A., Zeghal, M., Mercado, V.M. and El Shamy, U., 2013. Centrifuge and Large-Scale Modeling of Seismic Pore Pressures in Sands: Cyclic Strain Interpretation. *Journal of Geotechnical and Geoenvironmental Engineering*, 139(8), pp.1215–1234. https://doi.org/10.1061/(asce)gt.1943-5606.0000821.

Anderson, D., Cox, D., Mieras, R., Puleo, J.A. and Hsu, T., 2017. Observations of wave-induced pore pressure gradients and bed level response on a surf zone sandbar. *Journal of Geophysical Research: Oceans*, 122(6), pp.5169–5193. https://doi.org/10.1002/2016jc012557.

Chanson, H., 2006. Tsunami Surges on Dry Coastal Plains: Application of Dam Break Wave Equations. *Coastal Engineering Journal*, 48(4), pp.355–370. https://doi.org/10.1142/S0578563406001477.

Chen, M., Zheng, J., Tong, L., Zhang, J., Luo, M. and Chen, N., 2024. Experimental Study of Wave-Induced Pore Pressure Gradients around a Sandbar and Their Effects on Seabed Instability. *Journal of Marine Science and Engineering*, 12(9), p.1630. https://doi.org/10.3390/jmse12091630.

Dunn, S.L., Vun, P.L., Chan, A.H.C. and Damgaard, J.S., 2006. Numerical Modeling of Wave-Induced Liquefaction around Pipelines. *Journal of Waterway, Port, Coastal, and Ocean Engineering*, 132(4), pp.276–288. https://doi.org/10.1061/(asce)0733-950x(2006)132:4(276).

Fu, C., Wen, B., Lu, Y. and Zhao, T., 2025. Mathematical Modeling of Wave-Induced Pore Pressure Dynamics in Silty Seabeds. *JMSE*, 13(2), p.194. https://doi.org/10.3390/jmse13020194.

Ghosh, B. and Madabhushi, S.P.G., 2007. Centrifuge modelling of seismic soil structure interaction effects. *Nuclear Engineering and Design*, 237(8), pp.887–896. https://doi.org/10.1016/j.nucengdes.2006.09.027.

Ha, J.G., Lee, S.-H., Kim, D.-S. and Choo, Y.W., 2014. Simulation of soil–foundation–structure interaction of Hualien large-scale seismic test using dynamic centrifuge test. *Soil Dynamics and Earthquake Engineering*, 61–62, pp.176–187. https://doi.org/10.1016/j.soildyn.2014.01.008.

Hughes, S.A., 1993. *Physical Models and Laboratory Techniques in Coastal Engineering*. Advanced Series on Ocean Engineering. [online] WORLD SCIENTIFIC. https://doi.org/10.1142/2154.

Jeng, D.S., 2003. Wave-induced sea floor dynamics. *Applied Mechanics Reviews*, 56(4), pp.407–429. https://doi.org/10.1115/1.1577359.

Li, C., Gao, F. and Yang, L., 2021. Breaking-Wave Induced Transient Pore Pressure in a Sandy Seabed: Flume Modeling and Observations. *Journal of Marine Science and Engineering*, 9(2), p.160. https://doi.org/10.3390/jmse9020160.

MacRobert, C.J., Bernstein, G.S. and Nchabeleng, M.M., 2019. Dynamic Cone Penetrometer (DCP) Relative Density Correlations for Sands. *Soils and Rocks*, 42(2), pp.201–207. https://doi.org/10.28927/SR.422201.

Marry, M. and Foster, D., 2024. Field Observations of Hydrostatic Pressure Deviations in a Nearshore Sediment Bed. *Journal of Geophysical Research: Oceans*, 129(2), p.e2023JC019891. https://doi.org/10.1029/2023JC019891.

Michallet, H., Mory, M. and Piedra-Cueva, I., 2009. Wave-induced pore pressure measurements near a coastal structure. *Journal of Geophysical Research: Oceans*, 114(C6), p.2008JC005071. https://doi.org/10.1029/2008JC005071.

https://doi.org/10.9753/icce.v33.structures.78.

Mory, M., Michallet, H., Bonjean, D., Piedra-Cueva, I., Barnoud, J.M., Foray, P., Abadie, S. and Breul, P., 2007. A Field Study of Momentary Liquefaction Caused by Waves around a Coastal Structure. *Journal of Waterway, Port, Coastal, and Ocean Engineering*, 133(1), pp.28–38. https://doi.org/10.1061/(ASCE)0733-950X(2007)133:1(28).

Nguyen, A.D., 2023. Geo-centrifuge test in the evaluation behavior of soil-structure system under earthquake loading. *Vietnam Institute for Building Science and Technology*, 2023(vi.vol4), pp.3–10. https://doi.org/10.59382/j-ibst.2023.vi.vol4-1.

Paldor, A., Stark, N., Florence, M., Raubenheimer, B., Elgar, S., Housego, R., Frederiks, R.S. and Michael, H.A., 2022. Coastal topography and hydrogeology control critical groundwater gradients and potential beach surface instability during storm surges. *Hydrology and Earth System Sciences*, 26(23), pp.5987–6002. https://doi.org/10.5194/hess-26-5987-2022.

Sayedmasoud, M. and Ghayoomi, M., 2020. A semi-empirical model to predict excess pore pressure generation in partially saturated sand. *E3S Web of Conferences*, 195, p.02026. https://doi.org/10.1051/e3sconf/202019502026.

Scholtès, L., Chareyre, B., Michallet, H., Catalano, E. and Marzougui, D., 2015. Modeling wave-induced pore pressure and effective stress in a granular seabed. *Continuum Mechanics and Thermodynamics*, 27(1–2), pp.305–323. https://doi.org/10.1007/s00161-014-0377-2.

Seed, H.B. and Rahman, M.S., 1978. Wave-induced pore pressure in relation to ocean floor stability of cohesionless soils. *Marine Geotechnology*, 3(2), pp.123–150. https://doi.org/10.1080/10641197809379798.

Sriram, V., Didenkulova, I., Sergeeva, A. and Schimmels, S., 2016. Tsunami evolution and run-up in a large scale experimental facility. *Coastal Engineering*, 111, pp.1–12. https://doi.org/10.1016/j.coastaleng.2015.11.006.

Stark, N., 2017. Pore Pressure Response to Irregular Waves at a Sandy Beach. In: *Geotechnical Frontiers 2017*. [online] Geotechnical Frontiers 2017. Orlando, Florida: American Society of Civil Engineers. pp.409–417. https://doi.org/10.1061/9780784480472.043.

Terzaghi, K., Peck, R.B., Mesri, G. and Peck, R.B., 1996. *Soil mechanics in engineering practice*. 3. ed edn. New York: Wiley.

Xu, X., Xu, G., Yang, J., Xu, Z. and Ren, Y., 2021. Field observation of the wave-induced pore pressure response in a silty soil seabed. *Geo-Marine Letters*, 41(1), p.13. https://doi.org/10.1007/s00367-020-00680-6.

Young, Y.L., White, J.A., Xiao, H. and Borja, R.I., 2009. Liquefaction potential of coastal slopes induced by solitary waves. *Acta Geotechnica*, 4(1), pp.17–34. https://doi.org/10.1007/s11440-009-0083-6.

Zhang, J., Jiang, Q., Jeng, D., Zhang, C., Chen, X. and Wang, L., 2020. Experimental Study on Mechanism of Wave-Induced Liquefaction of Sand-Clay Seabed. *Journal of Marine Science and Engineering*, 8(2), p.66. https://doi.org/10.3390/jmse8020066.